

**Antimicrobial Peptide LL-37 on Surfaces Presenting
Carboxylate Anions**

Journal:	<i>Biomaterials Science</i>
Manuscript ID:	BM-ART-02-2015-000055.R1
Article Type:	Paper
Date Submitted by the Author:	30-Mar-2015
Complete List of Authors:	Qin, Guoting; The Methodist Hospital Research Institute, Lopez, Analette; University of Houston, Chemistry Santos, Catherine; University of Houston, Chemistry McDermott, Alison; University of Houston, College of Optometry Cai, Chengzhi; University of Houston, Chemistry

ARTICLE

Antimicrobial Peptide LL-37 on Surfaces Presenting Carboxylate Anions

Cite this: DOI: 10.1039/x0xx00000x

G. T. Qin,^{a,b} A. Lopez,^a C. Santos,^a A. M. McDermott,^b and C. Z. Cai*^aReceived 00th January 2012,
Accepted 00th January 2012

DOI: 10.1039/x0xx00000x

www.rsc.org/

Antimicrobial peptides (AMPs) are part of the immune system in a wide range of organisms. They generally carry positive charges under physiological conditions, allowing them to accumulate on the negatively charged bacterial membrane as the first step of bactericidal action. The concentration range of AMPs necessary for rapid killing of bacteria tested *in vitro* is much higher than levels found at epithelial surfaces and body fluids *in vivo*, and close to the a level that is toxic to the host cells. It is likely that AMPs *in vivo* are localized and act cooperatively to enhance antimicrobial activity, while the global concentration is low thus demonstrating low toxicity to host cells. Herein we employed well-defined mixed self-assembled monolayers (SAMs) to localize LL-37, one of the most studied AMPs, via electrostatic interactions. We systematically varied the surface density of LL-37, and found that the immobilized AMPs not only attracted bacteria *Pseudomonas aeruginosa* to the surface, but also killed nearly all bacteria when above a threshold density. More significantly, the AMPs displayed low toxicity to human corneal epithelial cells. The results indicated that localization of AMPs on suitable polyanion substrates facilitated the bactericidal activity while minimizing the cytotoxicity of AMPs.

Introduction

Antimicrobial peptides (AMPs) have a broad spectrum of antibacterial activity and a low susceptibility to development of bacterial resistance.¹ These much sought-after properties are associated with the fact that most AMPs are cationic and amphipathic, and target bacterial membranes with a relatively low binding affinity.^{2, 3} *In vitro* experiments show that a relatively high concentration of AMPs is needed to kill bacteria faster than their growth (bacteria may replicate themselves every 20 min).⁴ In this concentration range, however, AMPs often become toxic to host cells,⁴⁻⁷ which is one of the major hurdles for the development of AMP-based drugs.^{8, 9} Remarkably, the antimicrobial efficacy of AMPs is much higher *in vivo* than *in vitro*, suggesting the existence of a synergistic/cooperative effect *in vivo* to boost the antimicrobial activity and to reduce cytotoxicity. The mechanistic actions of AMPs have been extensively studied *in vitro*.¹⁰ In most studies, the polycationic AMPs are dissolved in a solution and interact with the negatively charged bacterial or artificial membranes, as illustrated in Figure 1A. In this case, a high concentration of AMPs is required to rapidly reach a threshold density on the bacterial membrane leading to lysis. Alternatively, the AMPs can be pre-localized on a scaffold or surface before interacting with bacteria as illustrated in Figure 1B and 1C. In this way, lower amounts but localized AMPs can still effectively disrupt the membrane. Immobilization of AMPs on surfaces has

attracted considerable interest relevant to the prevention of device-associated bacterial infections.^{4, 7, 11-29} The immobilized AMPs, especially those via a long, flexible linker attached to the C- or N-terminus, exhibited high antimicrobial activity.^{12, 28, 30-33} AMPs have also been attached onto water soluble scaffolds including nanoparticles,^{34, 35} soluble polymers,³⁶ micelles,³⁷⁻³⁹ hydrogel,⁴⁰ and liposomes.²⁸ The localization of AMPs onto these scaffolds resulted in moderate to large (2-18 fold) enhancement in the antimicrobial efficacy.

In comparison to covalent attachment, accumulation of AMPs onto scaffolds via non-covalent interactions has received less attention,⁴¹⁻⁴⁵ yet it is perhaps more relevant to the *in vivo* action of AMPs. Indeed, neutrophils can release neutrophil extracellular traps (NETs)⁴⁶⁻⁴⁸ that entrap bacteria and kill them with a high local concentration of antimicrobial proteins, such as histones. These polycationic protein molecules are accumulated through association with the extended polyanionic DNA backbones of the NETs.⁴⁹ While the mechanism of cationic antimicrobial peptide action in its free form in solution is well understood (Figure 1A), the antimicrobial mechanism while it is immobilized on the NETs is not. The majority of the previously reported systems in which AMPs were non-covalently immobilized were based on the layer-by-layer strategy,⁴²⁻⁴⁵ or incorporated into the polymer matrix.⁵⁰ These systems are not ideal for the study of the effect of AMP density on antimicrobial activity.

In this work we generated a better-defined model system to study the non-covalent immobilized AMPs. Specifically, we

immobilized the polycationic LL-37, one of the most studied human AMPs,^{8-10, 28, 51-60} on well-defined self-assembled monolayers (SAMs, Figure 1C) presenting carboxylate anions of various densities. As compared to the complex and heterogeneous *in vivo* systems and the layer-by-layer system, this model system allows quantification of the surface density of AMPs. We demonstrate that LL-37 can be stably immobilized on the carboxylate surfaces, and at a high density they rapidly kill nearly all *Pseudomonas aeruginosa* (PA, a common pathogenic Gram-negative bacterium) upon contact, while exhibiting low toxicity to human corneal epithelial cells.

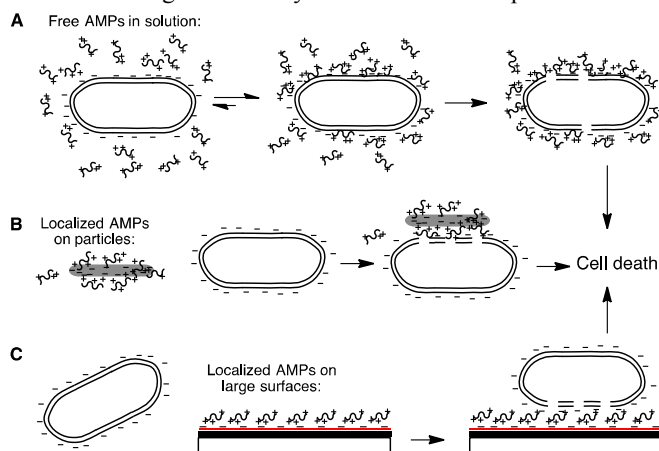


Figure 1. Illustration of a large number of AMP molecules in solution (A) and a small number of AMP molecules localized on micro- and nanoparticles or polymer scaffolds (B) and large solid substrate surfaces (C) for binding and disruption of anionic membranes of liposomes and bacteria.

Experimental

Materials. *N*-(17-hydroxy-3,6,9,12,15-pentaoxaheptadecyl)-16-mercaptohexadecanamide (**HS-OH**, Figure 2) and gold films deposited on silicon substrates were generous gifts from Prof. T. R. Lee at the University of Houston. 32-Mercapto-3,6,9,12,15,18,21-heptaaxadotriacontan-1-oic acid (**HS-COOH**, Figure 2, TRC biomedical research chemicals, Canada), carbenicillin (Sigma-Aldrich), and LL-37 (LLGDF-FRFSK-EKIGK-EFKRI-VQRIK-DFLRN-LVPRT-ES, Mw 4493.33 Da, from American Peptide Co., Sunnyvale, CA) were used directly. A *Pseudomonas aeruginosa* (PA) strain expressing green-fluorescent protein and a carbenicillin resistance gene (PAO1-GFP) was a generous gift from Dr. Alice Prince (Columbia University, NY). The SV40-transformed human corneal epithelial cells (HCECs) were received as a gift from Dr. Kaoru Araki-Sasaki (Tane Memorial Eye Hospital, Osaka, Japan). The components of an approximately 1 L of SHEM-X media used in the simultaneous monitoring of PAO1-GFP killing and HCEC cytotoxicity include 500 mL of Minimum Essential Medium Eagle (Sigma-Aldrich M4655), 500 mL of F12 Nutrient Mixture (1X) (Gibco 31765-035), 5 mL of dimethyl sulfoxide (Sigma-Aldrich D2650), 5 µg of bovine insulin (Sigma-Aldrich I1882), 100 µL of cholera toxin (Sigma-Aldrich C8052), 100 µL of epidermal growth factor (EGF) (Sigma-Aldrich) and 11.8 mL of HEPES buffer solution (1 M) (Gibco 15630-080).

Preparation of surfaces presenting LL-37. Silicon substrates with a gold film were cut into squares of $\sim 0.6 \times 0.6 \text{ cm}^2$ or $1.0 \times 0.6 \text{ cm}^2$, and washed with absolute ethanol. The samples were immediately immersed in a mixture of **HS-COOH** and **HS-OH** (molar ratios: 1:0, 1:1, 1:9, and 0:1, total concentration of **HS-**

COOH and **HS-OH**: 2 mM) in absolute ethanol for 20 h. The films were washed copiously with absolute ethanol, and dried with a flow of argon. Finally, 20 µL of LL-37 in PBS buffer (pH 7.4) with a final concentration of 83 µg/mL was used to fully cover each surface. The samples were allowed to incubate for 3 h in a sealed, humid compartment to avoid evaporation. The samples were washed with ethanol and water, and dried with a flow of argon.

X-ray photoelectron spectroscopy (XPS). A PHI 5700 X-ray photoelectron spectrometer, equipped with a monochromatic AlK α X-ray source ($h\nu = 1486.7 \text{ eV}$) at a take-off angle (TOA) of 45° from the film surface, was employed for XPS measurement. High-resolution XPS spectra were obtained by applying a window pass energy of 23.5 eV and the following numbers of scans: S2p, 30 scans; Au4f, 3 scans; C1s, 20 scans; O1s, 10 scans; N1s, 60 scans. The binding energy scales were referenced to the Au4f_{7/2} peak at 84.1 eV. XPS spectra were fitted with Gauss-Lorentz curve and the areas proportional to the atomic concentrations of each the elements were calculated using Phi Multipak V5.0A from Physical Electronics.

Ellipsometry. An ellipsometer (Rudolph Research, Auto EL III), operated with a 632.8 nm He-Ne laser at an incident angle of 70°, was employed for thickness measurement. The refractive index of the gold films was measured as 0.162. Several measurements were taken for each sample, and the mean values were reproducible within $\pm 1 \text{ \AA}$.

Surface plasma resonance (SPR) measurement. SPR measurements were conducted on an Autolab ESPRIT SPR (Eco Chemie, Utrecht, The Netherlands) equipped with a 670 nm laser and a 2-channel cuvette-system. Prior to each experiment, two SPR discs coated with a 50 nm gold film were cleaned with ethanol, and immediately immersed in a solution of **HS-COOH** (2 mM) or a mixture of **HS-OH/HS-COOH** (molar ratios: 9:1, total concentration: 2 mM) in ethanol overnight. The substrates were extensively washed with ethanol, and dried with a flow of argon. A 10 mM phosphate-buffered saline (PBS, 140 mM NaCl, pH 7.4, Sigma-Aldrich, MO) was used as running buffer for each experiment. The buffer was filtered through a 0.45-µm syringe filter followed by degassing with sonication for 5 min. Two SPR discs freshly coated with the same SAMs were loaded to the dual channel cuvette in the SPR instrument. The surfaces were washed at least two times with PBS buffer, each for 2 min, until a stable baseline was established. The binding experiments at different concentrations of freshly prepared LL-37 solution (16 µg/mL) in PBS buffer began by injection of 50 µL of a solution with a flow rate of 33 µL/min at 25 °C. The surface was then washed with PBS buffer for 2 h to monitor the dissociation of the peptide. Finally, the surface was washed with 0.3% (v/v) Triton X (Sigma-Aldrich), followed by PBS buffer until the baseline stabilized at 0 RU. Simultaneous SPR responses were measured in the dual channels, one for the binding measurement and the other for control in which only the running buffer was injected, and the difference in the SPR responses of the two channels were reported. Data analysis was performed with LMM Pro version 1.06 (Alfilisol LLC, Coventry, CT).

Antimicrobial activity of LL-37 on surfaces. One single isolated PAO1-GFP colony was used to inoculate 5 mL of LB with 300 µg/mL carbenicillin overnight at 37 °C. A bacterial suspension (1 mL) was used to inoculate 50 mL of fresh LB with 300 µg/mL carbenicillin, which was then incubated for 2 hours with vigorous shaking at 37 °C to achieve mid-log phase growth. Twenty-five milliliters of the warm PA culture were centrifuged at 3000 rpm for 10 minutes, and the bacterial cell

pellet was re-suspended in cold phosphate buffer (PB; 8.2 mM Na_2HPO_4 , 1.8 mM KH_2PO_4 (pH 7.4)). Optical density of the suspension was adjusted to 0.28 at 620 nm by adding an appropriate volume of PB. The bacterial suspension ($100\ \mu\text{L}$, approximately 10^8 cfu/mL) was used to fully cover the sample surfaces. After incubation at $37\ ^\circ\text{C}$ for 2 h without shaking, the substrates were taken out. One microliter of $15\ \mu\text{M}$ propidium iodide (PI) was placed on the substrate and covered by a cover slip and the sample was then inspected by fluorescence microscopy.

Fluorescence microscopy. Digital images were obtained using an Olympus BX 51 fluorescence microscope with a $60\times$ objective and Magnafire software, or a Nikon 80i fluorescence microscope with a $40\times$ objective and Elements software. Customized ImagePro software was used to count the number of bacterial cells, and to align and overlay the images.

In situ imaging of bacteria interacting with substrates presenting LL-37. Large pieces ($2\times 4\ \text{cm}^2$) of LL-37-presenting substrate were prepared as described above. A PAP Pen (Daido Sangyo, Co. Ltd. Tokyo) was used to draw a circle of $\sim 1\ \text{cm}$ in diameter on the surface. A droplet ($10\ \mu\text{L}$) of the bacterial solution in PB (10^8 cfu/mL) was added, followed by $1\ \mu\text{L}$ of PI inside the circle on the surface. A cover slip was placed on top of the circle, forming a sealed micro-chamber housing the bacteria on the LL-37 presenting surface. Fluorescence images were then taken at 3, 10, 30, and 60 min at the same area.

Preparation of SV40-transformed human corneal epithelial cells (HCECs). HCECs were maintained in 5 mL SHEM-X media with 10% fetal bovine serum (FBS) until 90-95% confluent in a 25 mL culture flask. The media was removed and the cells were washed with 2 mL of PBS. After removal of the PBS, 2 mL of 0.25% trypsin in EDTA was added. After incubation for 10 minutes, 8 mL of SHEM-X media was added to the media. The cell suspension was centrifuged for 2 minutes. The liquid was removed and the cell pellet was resuspended in 3 mL of SHEM-X without FBS and antibiotics.

Simultaneously monitoring the killing of PA and toxicity to HCECs in SHEM-X culture media on surfaces presenting LL-37. PAO1-GFP was prepared as described above except that the bacterial pellet was resuspended in SHEM-X without FBS and antibiotics. Fifty microliters of HCEC suspension was dropped on top of the LL-37 surface followed by $50\ \mu\text{L}$ of the PAO1-GFP suspension. After 90 minutes at room temperature, the substrates were taken out and $1\ \mu\text{L}$ of $15\ \mu\text{M}$ PI was added to the surface. The surface was covered by a cover slip and the sample was immediately viewed with a Nikon 80i fluorescence microscope with a $40\times$ objective. Images were obtained in bright-field, and with FITC and TRITC filters, and processed with NIS Elements software. For imaging of cells alone, $100\ \mu\text{L}$ of cell suspension was placed on top of the LL-37 surface.

Results and discussion

The SAMs **1a–4a** (Figure 2) were prepared from the COOH-terminated thiol **HS-COOH** and the inert thiol **HS-OH** of varied ratios on gold surfaces. They were characterized by X-ray photoelectron spectroscopy (XPS) and ellipsometry.

The XPS narrow scan in the $\text{C}1\text{s}$ region of the SAM **1a** (Figure 3a, blue curve) showed the emissions at 285.5, 287.0, and 288.8 eV, which were assigned to the alkyl (C-C), the etheric (C-O), and the carbonyl (C=O) carbons, respectively. The $\text{C-C}/\text{C-O}/\text{COOH}$ ratio of the SAM **1a** was 1:1.4:0.2, similar to the ratio of 1:1.4:0.1 for **HS-COOH**. Upon treatment with LL-37 to form the film **1b** (Figure 2) the signal intensity at

285.5 (C-C) and 288.8 eV (C=O) increased (Figure 3a, red curve). Also, a $\text{N}1\text{s}$ signal appeared at 401.0 eV (Figure 3b, red curve), which was absent in the SAM **1a** (Figure 3b, blue curve). The orange curve in Figure 3b shows the $\text{N}1\text{s}$ signal for the film **4a** that contains an amide linkage. Negligible amounts of LL-37 adhered to this neutral surface, as indicated by the overlapping of $\text{N}1\text{s}$ signals for the film **4a** before and after treatment with LL-37 (Figure 3b, orange and green curves). The result indicates that LL-37 with a net charge of +6 binds onto the COOH surfaces mainly via electrostatic interactions.

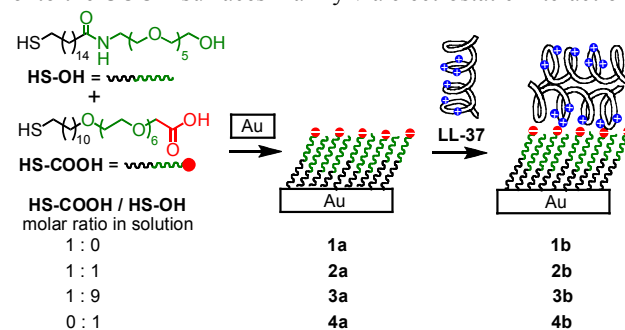


Figure 2. Immobilization of LL-37 via electrostatic interaction on the (mixed) SAMs **1a–4a** derived from **HS-OH** and **HS-COOH** with varied ratios on Au to form LL-37-presenting surfaces **1b–4b**.

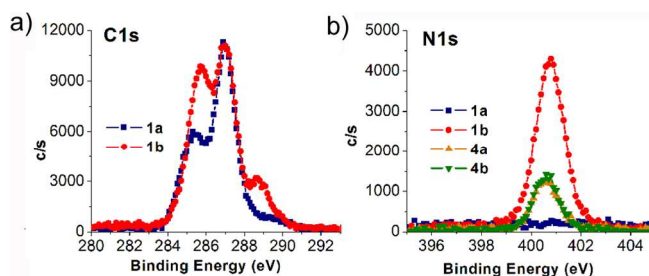


Figure 3. $\text{C}1\text{s}$ (a) and $\text{N}1\text{s}$ (b) XPS spectra of the SAMs **1a & 1b** and **4a & 4b**.

In physiological conditions, LL-37 molecules form α -helices where the charged and polar residues populate one side, while the hydrophobic residues cluster in the opposite side.^{9, 10, 52, 54-57, 61, 62} High salt concentrations promote self-assembly of the amphipathic helices into bundles with the hydrophobic side oriented inward and the polar side outward. To similarly maximize the electrostatic and hydrophobic interactions, the amphipathic molecules may self-assemble to form a bilayer on the COOH surfaces as illustrated in Figure 2. In the bilayer, the hydrophobic sides of the molecules are sandwiched between the polar sides of the bottom and top layers, which bind to the carboxylate surface and interact with the solution, respectively. Although further verification is needed, this bilayer model is supported by the following thickness and density data.

The surface densities of LL-37 were derived from the ellipsometric thickness and XPS data (Table 1). Upon adsorption of the peptide on the COOH surface **1a**, the thickness was increased by $12.5\ \text{\AA}$. Assuming a close packing, this thickness corresponds to a peptide density of $\sim 2.6\times 10^{13}/\text{cm}^2$ (Supplementary Information). A similar density of $3.3\times 10^{13}/\text{cm}^2$ was derived from the C/N ratio measured by XPS. Assuming an average width of $\sim 10\ \text{\AA}$, the lateral cross-section of the LL-37 helix is $\sim 550\ \text{\AA}^2$,⁶³ corresponding to a density of $3.6\times 10^{13}/\text{cm}^2$ for a bilayer of the peptide, which is similar to the measured values. The thickness ($\sim 12.5\ \text{\AA}$) of the

film was only slightly greater than twice the width ($\sim 5 \text{ \AA}$) of the helical backbone, probably because the side chains of the helix tend to orient laterally. Note that the above bilayer helical structure illustrated in Figure 2 represents only one of the possible structures that would agree with the measured thickness and XPS data. Other characterization such as photon polarization modulation infrared reflection absorption spectroscopy (PMIRRAS) measurements is necessary to shed light on the structure of the immobilized peptide, but is beyond the scope of this study. A similar peptide density (Table 1) was obtained on the $\sim 80\%$ COOH surface **2a**. This result is expected due to the abundance of underlying COOH groups (Table S2) for interacting with the peptide.

Table 1. Ellipsometric thickness of LL-37 ($T_{\text{LL-37}}$) on the (mixed) SAMs **1a–4a** with varied density of COOH groups and the surface density derived from thickness ($^T N_{\text{LL-37}}/\text{cm}^2$) and XPS ($^{\text{XPS}} N_{\text{LL-37}}/\text{cm}^2$)^[a]

SAM	$T_{\text{LL-37}}$ (\AA)	$^T N_{\text{LL-37}}/\text{cm}^2$ ^[a]	$^{\text{XPS}} N_{\text{LL-37}}/\text{cm}^2$ ^[a]
1a (100% COOH)	12.5 ± 0.9	2.6×10^{13}	3.3×10^{13}
2a ($\sim 80\%$ COOH) ^[a]	10.7 ± 2.6	2.2×10^{13}	3.1×10^{13}
3a ($\sim 2\%$ COOH) ^[a]	0.8 ± 1.5	1.7×10^{12}	6.6×10^{12}
4a (0% COOH)	-1.9 ± 0.6	0	0

[a] For details on deriving the COOH and peptide densities from the XPS and ellipsometric data, see Tables S1 and S2 in Supplementary Information.

The binding of LL-37 (16 $\mu\text{g}/\text{mL}$ in PBS) to the 100% COOH surfaces **1a** and $\sim 2\%$ COOH surfaces **3a** was monitored *in situ* by surface plasmon resonance (SPR, Figure 4). The SPR response, increasing with the adsorption of LL-37, rapidly reached a maximum. Following the rapid binding of LL-37 on the surfaces **1a** and **3a**, a slow desorption occurred (Figure 4a,b), probably due to the reorganization of the peptides to maximize the binding, which may lead to secretion of some of the initially weakly adsorbed molecules. Upon washing with PBS, there was a rapid drop in SPR response due to the change of dielectric constants, but the immobilized LL-37 on both films did not desorb under a continuous flow of PBS for 2 hours, as shown by the constant SPR response (Figure 4c,d). The tightly bound peptide could be removed by sodium dodecyl sulfate solution to regenerate the COOH surface.

This result is remarkable, especially for the $\sim 2\%$ COOH surface **3a**. As compared to the amount of peptide adsorbed onto the 100% COOH surface **1a**, the peptide adsorption on this surface was decreased to about 20% (Table 1), which was still much less than the deduction of surface COOH groups ($\sim 2\%$ vs 100%). We attribute the observed high stability of LL-37 on this surface to the presence of nano-domains consisting of a high density of COOH groups. Such nano-domains of COOH groups due to self-assembly on similar mixed SAMs was previously reported. The high local density of COOH on the nano-domains allows strong binding of the peptide, although the average global density of the peptide is low. Significantly, the immobilized peptide on both surfaces remained stable in the presence of polyanionic LPS from the outer membrane of Gram-negative bacteria. Only a slight decrease of SPR response, likely due to the change of dielectric constants, was recorded upon addition of up to 1 mg/mL of LPS solutions (Figure 4).

The antibacterial activity of the adsorbed LL-37 was then evaluated using a strain of PA expressing green fluorescent protein (PAO1-GFP) with propidium iodide (PI) used as the viability indicator in fluorescent imaging of this bacterial strain.^{64, 65} As an example, Figure 5 shows that while all

bacteria fluoresce green (Figure 5a), those with compromised membranes also fluoresce red (Figure 5b) due to the formation of PI-DNA complexes upon internalization of PI through the membrane-compromised cells. Figure 5c is the overlay of the two images, clearly revealing a small population of the intact bacteria (green) among the PI-positive bacteria (orange).

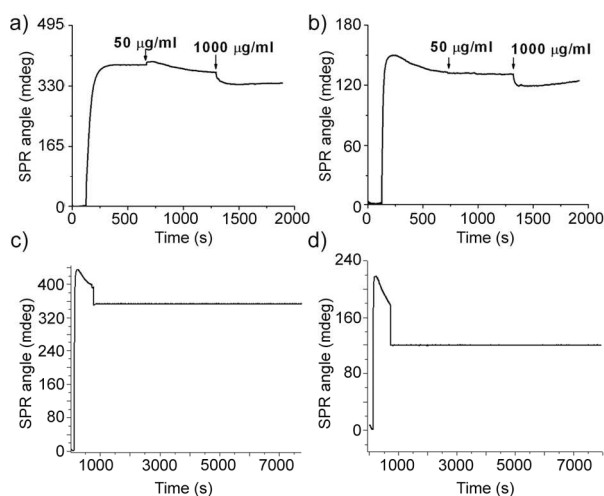


Figure 4. SPR sensorgrams monitoring the adsorption of LL-37 (16 $\mu\text{g}/\text{mL}$ for a,b, and 32 $\mu\text{g}/\text{mL}$ for c,d) on the 100% COOH surface **1a** (a) and the $\sim 2\%$ COOH surface **3a** (b) in 10 mM PBS, and the desorption of the peptide upon injection of LPS at 50 $\mu\text{g}/\text{mL}$ and then at 1 mg/mL in PBS (a,b), and continuous washing with PBS for 2 h for the above treated surface **1a** (c) and surface **3a** (d).

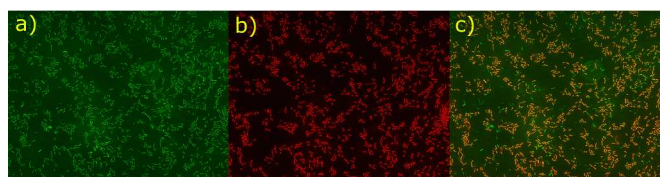


Figure 5. Representative fluorescence images of PAO1-GFP on surfaces presenting LL-37 (in this case, surface **1b**, Figure 2), obtained with a FITC filter showing all adsorbed PA (a) and with a TRITC filter showing the membrane-compromised PA (b) on the same area ($100 \times 100 \mu\text{m}^2$), and the overlay (c), revealing the PI-negative bacteria (in green) among the PI-positive bacteria (in orange). Among all bacteria fluorescing green (a), those with compromised membranes also fluoresce red (b).

Figure 6 plots the density of the adsorbed bacteria and among them the membrane-compromised (PI-positive) bacteria as a function of the surface density of LL-37. Remarkably, the data show that a higher density of LL-37 not only increased the binding of bacteria onto the surface but also the killing of them. The antibacterial efficacy is defined as the number of PI-positive bacteria over the number of all adsorbed bacteria. Thus, surface **1b** showed significant killing ($\sim 97\%$) while surfaces **2b** and **3b** only exhibited $\sim 65\%$ and $\sim 20\%$ killing of the bacteria, respectively. Higher density of LL-37 captures more bacteria, likely due to the presence of more positive charge on the surface leading to a stronger electrostatic interaction with the Gram-negative bacteria, which also contributes to its higher bactericidal activity. Also, all bacteria that adsorbed on the OEG surfaces (**4a**) in the absence of LL-37 survived. Significantly, there was a steep increase of efficacy when the density of LL-37 exceeded $\sim 3 \times 10^{13}$ molecules/ cm^2 . This result suggests that beyond this critical density, LL-37 molecules could act cooperatively to facilitate the bactericidal action. However, it should be noted that LL-37 might be

gradually removed by the bacteria. Although the SPR results did not show any desorption of LL-37 on all COOH-presenting surfaces in 0.1% LPS, the high local concentration of the polyanionic LPS on the bacterial outer membrane may facilitate their removal. Evaluating the possibility of LL-37 desorption during interaction with the bacteria, *e.g.*, using radioactive isotope labelling of the peptide, is out of the scope of this article.

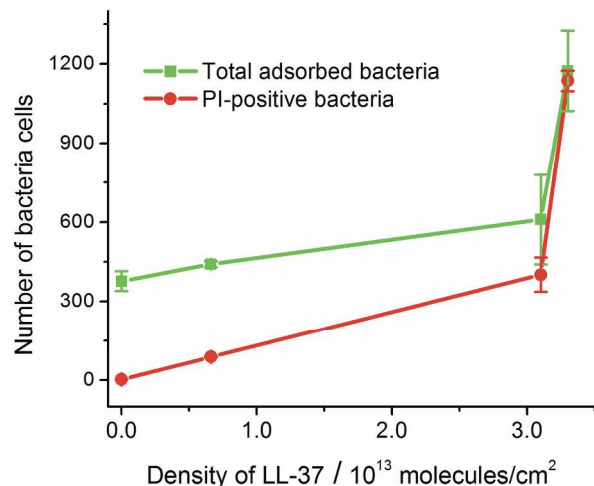


Figure 6. Plot of the total number of bacteria (green) and among them the number of PI-positive bacteria (red) on the field of view ($100 \times 100 \mu\text{m}^2$), which were adsorbed on surfaces presenting LL-37 of various densities derived from XPS data. Data were obtained at 2 h after treatment of the films with a bacterial suspension (10^8 cfu/mL), and are expressed as mean number of bacteria \pm standard deviation of three experiments. The substrates ($\sim 1.0 \times 0.6 \text{ cm}^2$) were fully covered by $100 \mu\text{L}$ of $\sim 10^8$ cfu/mL bacteria suspension. Hence the high density peptide surface **1b** captured most (>70%) of the bacteria in the solution.

Real time fluorescence images in Figure 7 revealed that the membrane-disruption of the adhered bacteria occurred as early as 3 min (time needed for imaging) after addition of the bacterial culture to the surfaces. Increasing numbers of bacteria adhered onto the surface overtime. We observed the disappearance of membrane-compromised bacteria (PI-positive, indicated by the green arrows in Figure 7) and adsorption of new bacteria (indicated by the white arrows). Increasing red fluorescence was observed in the bulk solution overtime, indicating an increase amount of lysed or membrane-disrupted bacteria in the solution.

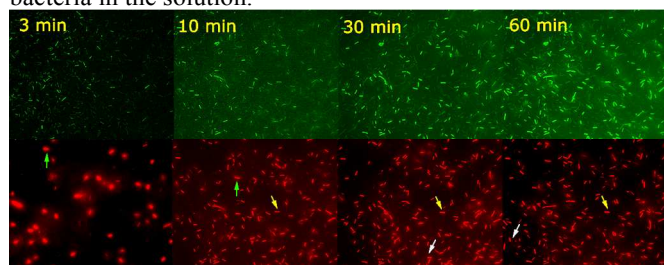


Figure 7. Representative fluorescence images of PAO1-GFP adsorbed on the LL-37-presenting surface **1b** at 3, 10, 30, and 60 min. The green images show all adsorbed bacteria, and the corresponding red images show the membrane-compromised bacteria. Examples of the bacteria cells that were newly absorbed, disappeared, and stayed over time are indicated by white, green, and yellow arrows, respectively.

To probe the toxicity of the immobilized LL-37, we incubated a mixture of SV40-transformed human corneal

epithelial cells (SV40-HCEC),¹⁸ the bacteria and the indicator PI in SHEM-X media on the LL-37 presenting surfaces **1a** for 90 min. Bright field and fluorescence images (Figure 8 and Figure S2) show substantial coverage of the surface by the bacteria, and over 90% of them were membrane compromised. Significantly, the SV40-HCECs remained alive (membrane not compromised). Note that most of the SV40-HCECs in Figure 8 were in contact with the surface (although had not yet spread), as indicated by the bright field images (see Figure S2) focused on the film surface. Dead bacteria are also visible with the SV40-HCECs.

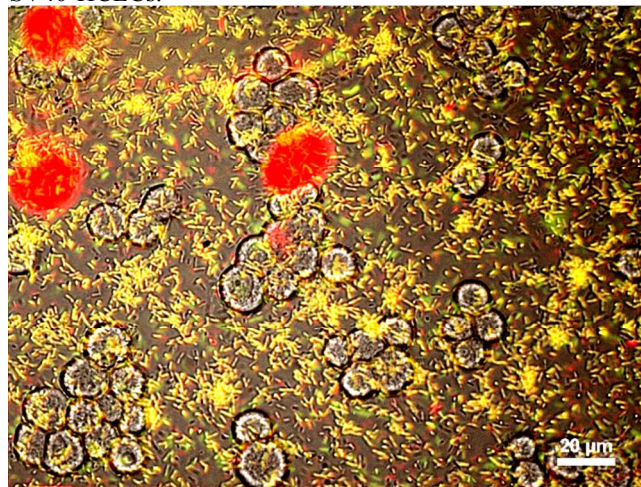


Figure 8. A representative overlay of a reflected bright field and fluorescence images of PAO1-GFP and SV40-HCECs incubated in SHEM-X media on the LL-37-presenting surface **1b** in the presence of PI. The original images before overlaying are given in Figure S2. The images were taken after 90 minutes of incubation.

Conclusions

In conclusion, using a well-defined model system we have demonstrated that proper localization of AMPs on polyanionic surfaces results in a high bactericidal efficacy and a low cytotoxicity to host cells. The bactericidal efficacy of the immobilized LL-37 steeply increased when its surface density was above a threshold value ($\sim 3 \times 10^{13}$ molecules/cm²). Notably, the *in vivo* systems contain substantial amounts of polyanionic aggregates, including LPS and DNA from bacteria and host cells. Our result highlights the need to investigate the antimicrobial properties and cytotoxicity of AMPs immobilized on the surface of these polyanionic aggregates for better understanding their actions *in vivo*.

Acknowledgements

This work was supported by NSF grants DMR-0706627 and DMR-1207583, The Welch Foundation grant E-1498, and NIH grants R21EY018303 and EY13175. We thank Prof. R. Advincula for allowing use of the SPR.

Notes and references

^a Department of Chemistry, University of Houston, Houston, Texas 77204, USA.

^b The Ocular Surface Institute, College of Optometry, University of Houston, Houston, Texas 77204, USA.

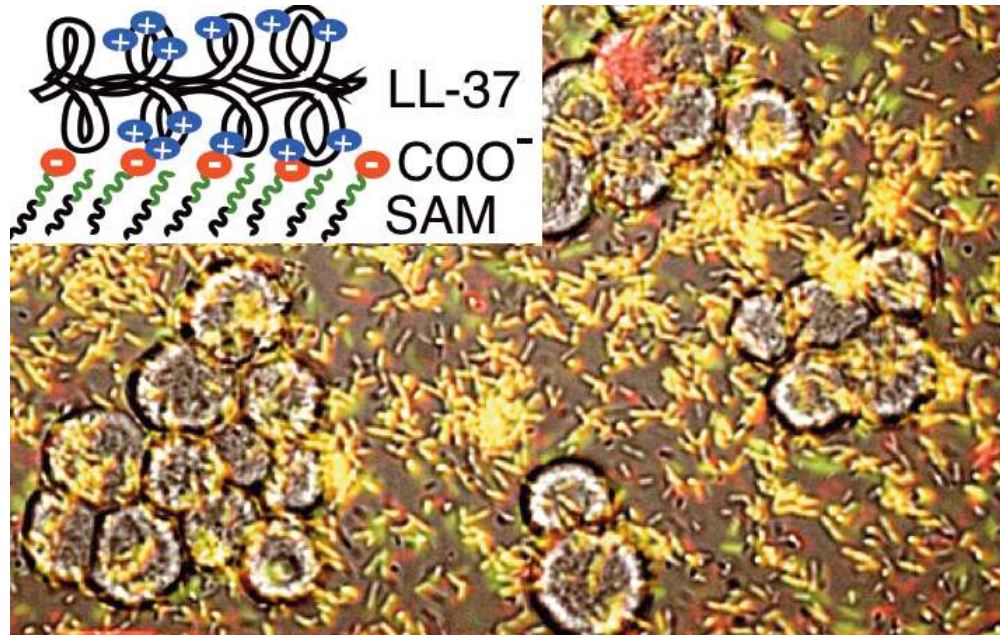
† Electronic Supplementary Information (ESI) available: [LL-37 surface density estimation from ellipsometry thickness and XPS data, and

antimicrobial efficacy and cytotoxicity of LL-37 surfaces]. See 32
DOI: 10.1039/b000000x/

References

- 1 R. E. W. Hancock and H. G. Sahl, *Nat. Biotechnol.*, 2006, **24**, 1551.
- 2 A. Peschel and H. G. Sahl, *Nat. Rev. Microbiol.*, 2006, **4**, 529.
- 3 J. G. Hurdle, A. J. O'Neill, I. Chopra and R. E. Lee, *Nat. Rev. Microbiol.*, 2011, **9**, 62.
- 4 L. C. Huang, T. D. Petkova, R. Y. Reins, R. J. Proske and A. M. McDermott, *Investigative Ophthalmology & Visual Science*, 2006, **47**, 2369.
- 5 C. D. Ciornei, T. Sigurdardottir, A. Schmidtchen and M. Bodelsson, *Antimicrobial Agents and Chemotherapy*, 2005, **49**, 2845.
- 6 J. Aarbiou, G. S. Tjabringa, R. M. Verhoosel, D. K. Ninaber, S. R. White, L. T. C. Peltenburg, K. F. Rabe and P. S. Hiemstra, *Inflamm. Res.*, 2006, **55**, 119.
- 7 A. M. McDermott, *Experimental Eye Research*, 2013, **117**, 53.
- 8 C. R. Brandt, *J. Ocular Pharmacol. Ther.*, 2014, **30**, 691.
- 9 Y. J. Gordon, E. G. Romanowski and A. M. McDermott, *Curr. Eye Res.*, 2005, **30**, 505.
- 10 A. M. McDermott, *Ophthalmic Res.*, 2009, **41**, 60.
- 11 S. A. Onaizi and S. S. J. Leong, *Biotechnology Advances*, 2011, **29**, 67.
- 12 M. Gabriel, K. Nazmi, E. C. Veerman, A. V. N. Amerongen and A. Zentner, *Bioconjugate Chemistry*, 2006, **17**, 548.
- 13 K. Glinel, A. M. Jonas, T. Jouenne, J. Leprince, L. Galas and W. T. S. Huck, *Bioconjugate Chemistry*, 2009, **20**, 71.
- 14 V. Humblot, J. F. Yala, P. Thebault, K. Boukerma, A. Hequet, J. M. Berjeaud and C. M. Pradier, *Biomaterials*, 2009, **30**, 3503.
- 15 P. Appendini and J. H. Hotchkiss, *J. Appl. Polym. Sci.*, 2001, **81**, 609.
- 16 M. Bagheri, M. Beyermann and M. Dathe, *Antimicrobial Agents and Chemotherapy*, 2009, **53**, 1132.
- 17 W. M. Cho, B. P. Joshi, H. Cho and K. H. Lee, *Bioorg. Med. Chem. Lett.*, 2007, **17**, 5772.
- 18 S. L. Haynie, G. A. Crum and B. A. Doele, *Antimicrobial Agents and Chemotherapy*, 1995, **39**, 301.
- 19 K. Hilpert, M. Elliott, H. Jenssen, J. Kindrachuk, C. D. Fjell, J. Komer, D. F. H. Winkler, L. L. Weaver, P. Henklein, A. S. Ulrich, S. H. Y. Chiang, S. W. Farmer, N. Pante, R. Volkmer and R. E. W. Hancock, *Chem. Biol.*, 2009, **16**, 58.
- 20 M. D. P. Willcox, E. B. H. Hume, Y. Aliwarga, N. Kumar and N. Cole, *J. Appl. Microbiol.*, 2008, **105**, 1817.
- 21 M. D. Steven and J. H. Hotchkiss, *J. Appl. Polym. Sci.*, 2008, **110**, 2665.
- 22 M. Bagheri, M. Beyermann and M. Dathe, *Bioconjugate Chemistry*, 2012, **23**, 66.
- 23 A. Hequet, V. Humblot, J. M. Berjeaud and C. M. Pradier, *Colloids and Surfaces B-Biointerfaces*, 2011, **84**, 301.
- 24 J. B. D. Green, T. Fulghum and M. A. Nordhaus, *Biointerphases*, 2011, **6**, MR13.
- 25 D. Alves and M. O. Pereira, *Biofouling*, 2014, **30**, 483.
- 26 D. Dutta and M. D. P. Willcox, *Eye Contact Lens-Sci. Clin. Pra.*, 2014, **40**, 312.
- 27 H. Etayash, L. Norman, T. Thundat, M. Stiles and K. Kaur, *Acs Applied Materials & Interfaces*, 2014, **6**, 1131.
- 28 A. Kumar, S. S. Kolar, M. R. Zao, A. M. McDermott and C. Z. Cai, *Molecular Biosystems*, 2011, **7**, 711.
- 29 S. Y. Hou, C. H. Zhou, Z. G. Liu, A. W. Young, Z. H. Shi, D. C. Ren and N. R. Kallenbach, *Bioorg. Med. Chem. Lett.*, 2009, **19**, 5478.
- 30 X. Chen, H. Hirt, Y. P. Li, S. U. Gorr and C. Aparicio, *Plos One*, 2014, **9**, 8.
- 31 D. M. Eby, K. E. Farrington and G. R. Johnson, *Biomacromolecules*, 2008, **9**, 2487.
- Y. Li, C. M. Santos, A. Kumar, M. R. Zhao, A. I. Lopez, G. T. Qin, A. M. McDermott and C. Z. Cai, *Chemistry-a European Journal*, 2011, **17**, 2656.
- C. M. Santos, A. Kumar, W. Zhang and C. Z. Cai, *Chemical Communications*, 2009, DOI: 10.1039/b821148e, 2854.
- S. Leptihn, J. Y. Har, J. Z. Chen, B. Ho, T. Wohland and J. L. Ding, *BMC Biol.*, 2009, **7**, 13.
- S. Ruden, K. Hilpert, M. Berditsch, P. Wadhvani and A. S. Ulrich, *Antimicrobial Agents and Chemotherapy*, 2009, **53**, 3538.
- J. H. Zhang, D. A. Kissounko, S. E. Lee, S. H. Gellman and S. S. Stahl, *J. Am. Chem. Soc.*, 2009, **131**, 1589.
- M. L. Becker, J. Q. Liu and K. L. Wooley, *Biomacromolecules*, 2005, **6**, 220.
- L. H. Liu, K. J. Xu, H. Y. Wang, P. K. J. Tan, W. M. Fan, S. S. Venkatraman, L. J. Li and Y. Y. Yang, *Nat. Nanotechnol.*, 2009, **4**, 457.
- H. Y. Wang, K. J. Xu, L. H. Liu, J. P. K. Tan, Y. B. Chen, Y. T. Li, W. M. Fan, Z. Q. Wei, J. F. Sheng, Y. Y. Yang and L. J. Li, *Biomaterials*, 2010, **31**, 2874.
- R. T. C. Cleophas, M. Riool, H. C. Q. van Ufford, S. A. J. Zaat, J. A. W. Kruijtzter and R. M. J. Liskamp, *ACS Macro Lett.*, 2014, **3**, 477.
- G. Cado, R. Aslam, L. Seon, T. Garnier, R. Fabre, A. Parat, A. Chassepot, J. C. Voegel, B. Senger, F. Schneider, Y. Frere, L. Jiery, P. Schaaf, H. Kerdjoudj, M. H. Metz-Boutigue and F. Boulmedais, *Advanced Functional Materials*, 2013, **23**, 4801.
- O. Etienne, C. Picart, C. Taddei, Y. Haikel, J. L. Dimarq, P. Schaaf, J. C. Voegel, J. A. Ogier and C. Egles, *Antimicrobial Agents and Chemotherapy*, 2004, **48**, 3662.
- A. Guyomard, E. De, T. Jouenne, J. J. Malandain, G. Muller and K. Glinel, *Advanced Functional Materials*, 2008, **18**, 758.
- J. S. Rudra, K. Dave and D. T. Haynie, *J. Biomater. Sci.-Polym. Ed.*, 2006, **17**, 1301.
- A. Shukla, K. E. Fleming, H. F. Chuang, T. M. Chau, C. R. Loose, G. N. Stephanopoulos and P. T. Hammond, *Biomaterials*, 2010, **31**, 2348.
- V. Brinkmann, U. Reichard, C. Goosmann, B. Fauler, Y. Uhlemann, D. S. Weiss, Y. Weinrauch and A. Zychlinsky, *Science*, 2004, **303**, 1532.
- V. Brinkmann and A. Zychlinsky, *Nat. Rev. Microbiol.*, 2007, **5**, 577.
- M. Zawrotniak and M. Rapala-Kozik, *Acta Biochimica Polonica*, 2013, **60**, 277.
- F. Wartha, K. Beiter, S. Normark and B. Henriques-Normark, *Current Opinion in Microbiology*, 2007, **10**, 52.
- P. A. Fulmer, J. G. Lundin and J. H. Wynne, *Acs Applied Materials & Interfaces*, 2010, **2**, 1266.
- R. Bucki, F. J. Byfield and P. A. Janmey, *Eur. Resp. J.*, 2007, **29**, 624.
- R. Bucki, A. G. Sostarecz, F. J. Byfield, P. B. Savage and P. A. Janmey, *Journal of Antimicrobial Chemotherapy*, 2007, **60**, 535.
- M. F. Burton and P. G. Steel, *Natural Product Reports*, 2009, **26**, 1572.
- U. H. N. Durr, U. S. Sudheendra and A. Ramamoorthy, *Biochim. Biophys. Acta-Biomembr.*, 2006, **1758**, 1408.
- S. Sandgren, A. Wittrup, F. Cheng, M. Jonsson, E. Eklund, S. Busch and M. Belting, *J. Biol. Chem.*, 2004, **279**, 17951.
- J. X. Tang, Q. Wen, A. Bennett, B. Kim, C. A. Sheils, R. Bucki and P. A. Janmey, *Am. J. Physiol.-Lung Cell. Mol. Physiol.*, 2005, **289**, L599.
- G. S. Wang, *J. Biol. Chem.*, 2008, **283**, 32637.
- K. K. Cherreddy, C. H. Her, M. Comune, C. Moia, A. Lopes, P. E. Porporato, J. Vanacker, M. C. Lam, L. Steintraesser, P. Sonveaux, H. J. Zhu, L. S. Ferreira, G. Vandermeulen and V. Preat, *J. Control. Release*, 2014, **194**, 138.
- M. Vignoni, H. D. A. Weerasekera, M. J. Simpson, J. Phopase, T. F. Mah, M. Griffith, E. I. Alarcon and J. C. Scaiano, *Nanoscale*, 2014, **6**, 5725.
- R. Lande, E. Botti, C. Jandus, D. Dojcinovic, G. Fanelli, C. Conrad, G. Chamilos, L. Feldmeyer, B. Marinari, S. Chon, L. Vence, V. Riccieri, P. Guillaume, A. A. Navarini, P. Romero, A. Costanzo, E. Piccolella, M. Gilliet and L. Frasca, *Nat. Commun.*, 2014, **5**, 15.

- 61 G. Wang, *Pharmaceuticals*, 2014, **7**, 545.
- 62 X. Li, Y. Li, H. Han, D. W. Miller and G. Wang, *Journal of the American Chemical Society*, 2006, **128**, 5776.
- 63 F. Neville, M. Cahuzac, O. Kononov, Y. Ishitsuka, K. Y. C. Lee, I. Kuzmenko, G. M. Kale and D. Gidalevitz, *Biophysical Journal*, 2006, **90**, 1275.
- 64 M. R. Benoit, C. G. Conant, C. Ionescu-Zanetti, M. Schwartz and A. Matin, *Applied and Environmental Microbiology*, 2010, **76**, 4136.
- 65 K. Lim, R. R. Y. Chua, R. Saravanan, A. Basu, B. Mishra, P. A. Tarnbyah, B. Ho and S. S. J. Leong, *Acs Applied Materials & Interfaces*, 2013, **5**, 6412.



Non-covalently immobilized antimicrobial peptide LL-37 attracts and rapidly kills bacteria upon contact
60x38mm (300 x 300 DPI)